Properties of evanescent waves in anisotropic media

Ilya Tsvankin
Center for Wave Phenomena, Department of Geophysics, Colorado School of Mines, Golden, CO 80401-1887, USA

ABSTRACT
Evanescent (inhomogeneous) waves contained in the plane-wave decomposition of point-source radiation produce not only surface waves but also nongeometrical modes that can be recorded far away from the boundary. This paper gives an analytic description of evanescent P-, SV-, and SH-waves propagating in the symmetry planes of transversely isotropic and orthorhombic media.
Simple weak-anisotropy approximations for the slowness and polarization vectors of horizontally traveling evanescent waves are obtained by linearizing the Christoffel equation in the anisotropy parameters. While both the horizontal slowness (m_1) and the imaginary part of the vertical slowness (m_3) can take a wide range of values, the relationship between them (i.e., between the horizontal velocity and the vertical decay factor) is controlled by the stiffness matrix. For P-waves, this relationship is sensitive even to relatively small values of the Thomsen parameters δ and, especially, ϵ. The weak-anisotropy approximation correctly reproduces the trend of the P-wave function $m_1(m_3)$ for moderately anisotropic media, but deteriorates with increasing difference between ϵ and δ, as the model deviates from elliptical. The anisotropic terms in the dependence of m_1 on m_3 are particularly significant for the SV-wave because they include the parameter σ, which often exceeds 0.5. Anisotropy also distorts the particle motion of evanescent P- and SV-waves by changing the eccentricity of the polarization ellipse.
The results of this work can be used to develop asymptotic solutions for nongeometrical waves and design new anisotropic parameter-estimation algorithms for cross-hole and VSP surveys. In particular, measurements of the vertical decay factor of leaking waves traveling between boreholes can help to constrain the anisotropy parameters.

Key words: evanescent waves, slowness vector, polarization, weak-anisotropy approximation, anisotropic media, transverse isotropy

Introduction

A plane wave is called evanescent or inhomogeneous if at least one component of its slowness vector is complex. The imaginary part of the slowness vector causes spatial amplitude decay, with the planes of constant amplitude generally different from the planes of constant phase (i.e., from the wavefront). Evanescent waves are generated during reflection and transmission of conventional homogeneous plane waves if the angle of incidence exceeds the critical angle (e.g., Aki and Richards, 1980). Also, plane-wave decomposition of point-source radiation always includes a range of evanescent plane waves whose velocities change continuously between zero and the medium velocity (e.g., Brekhovskikh, 1980).

If the distance between the source and the nearest medium boundary is smaller than the predominant wavelength, evanescent energy contained in the point-source radiation excites surface (Rayleigh, Stoneley) waves. Furthermore, evanescent plane waves can be transformed into homogeneous (non-decaying) waves during the reflection/transmission process, giving rise to so-called "nongeometrical" or "nonray" modes.

For example, if a point pressure source is located

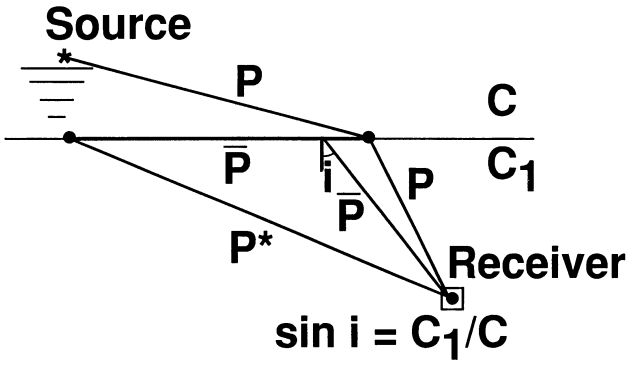

Figure 1. Asymptotic "raypaths" of the pseudospherical wave P* and leaking wave $\bar{\text{P}}$ generated at the boundary between two acoustic halfspaces with the velocities c and c_1 ($c > c_1$). The amplitudes of both nongeometrical waves decay between the source and the boundary. The traveltime of the $\bar{\text{P}}$-wave almost coincides with that of the conventional transmitted P-wave, while the wave P* forms a later arrival (after Tsvankin, 1995).

near a plane interface between two acoustic (fluid) media, the wavefield transmitted into the low-velocity halfspace contains two nongeometrical waves shown in Figure 1 (for a more detailed discussion, see Tsvankin, 1995). The wave P* is called "pseudospherical" because it has a spherical wavefront centered at the projection of the source onto the boundary. According to Snell's law, the P*-wave can exist only in the post-critical domain between the boundary and the critical angle $\theta_{\text{cr}} = \sin^{-1}(c_1/c)$. The second nongeometrical wave, $\bar{\text{P}}$, is a "leaking" mode similar to conventional head waves. It propagates along the boundary with a horizontal velocity slightly smaller than c and has a conical wavefront in the low-velocity halfspace. The take-off angle i for the $\bar{\text{P}}$-wave (Figure 1) is close to the critical angle θ_{cr}.

Nongeometrical waves from buried sources produce intensive secondary reflected and head waves and, unlike surface waves, can be recorded far away from the boundary (Tsvankin, 1995). Because of nongeometrical phenomena, P-wave sources excite several intensive shear modes, such as the pseudospherical wave S* (Hron and Mikhailenko, 1981) and leaking waves propagating with shear-wave velocities (Tsvankin, 1995). This shear-wave energy can be of particular importance to anisotropic parameter-estimation algorithms that require a combination of P- and S-wave data (Tsvankin, 2005). Whereas it is well known that anisotropy has a strong influence on surface waves (Crampin and Taylor, 1971; Crampin, 1975), existing results for nongeometrical waves are restricted to isotropic models. To give an analytic description of nongeometrical phenomena in anisotropic media, it is necessary to solve the wave equation for incident evanescent plane waves.

The goal of this paper is to build a foundation for the asymptotic analysis of nongeometrical modes in anisotropic media by obtaining closed-form expressions for the slowness and polarization components of evanescent waves. For simplicity, I consider plane waves with the slowness vector confined to a symmetry plane of transversely isotropic (TI) or orthorhombic media. Linearization of the relationship between the horizontal and vertical slownesses (i.e., between the velocity and amplitude decay factor) is used to identify the combinations of the anisotropy parameters responsible for the properties of evanescent waves. Numerical tests for typical TI models confirm the strong influence of anisotropy on the slowness vector of evanescent P-waves and help to evaluate the accuracy of the linearized solution.

Christoffel equation for evanescent waves

Let us consider a harmonic plane wave propagating in a homogeneous, arbitrarily anisotropic medium:

$$u_n = U_n \, e^{i\omega(m_j x_j - t)} \,, \tag{1}$$

where $\mathbf{u}$ is the displacement vector, $\mathbf{U}$ is the unit polarization vector, ω is the angular frequency, and $\mathbf{m}$ is the slowness vector. If at least one of the components of the slowness vector is complex and

$$m_n = m_n^{\text{re}} + i m_n^{\text{im}} \,, \tag{2}$$

the wave is called evanescent or inhomogeneous:

$$u_n = U_n \, e^{i\omega(m_j^{\text{re}} x_j - t) - \omega m_j^{\text{im}} x_j} \,. \tag{3}$$

To obtain the velocity, polarization, and amplitude decay factor of evanescent waves, the plane wave from equation 3 should be substituted into the wave equation,

$$\rho \, \frac{\partial^2 u_i}{\partial t^2} - c_{ijkl} \, \frac{\partial^2 u_k}{\partial x_j \, \partial x_l} = 0 \,. \tag{4}$$

Here, ρ is the density and c_{ijkl} is the stiffness tensor, which is assumed to be real (i.e., the medium is non-attenuative); summation over repeated indices is implied. This substitution results in the Christoffel equation, which has the same form as that for conventional homogeneous waves (e.g., Helbig, 1994; Tsvankin, 2005):

$$[c_{ijkl} \, m_j \, m_l - \rho \delta_{ik}] \, U_k = 0 \,, \tag{5}$$

where $c_{ijkl} \, m_j \, m_l$ is usually called the Christoffel matrix (G_{ik}) and δ_{ik} is Kronecker's symbolic δ. For evanescent waves, both the slowness and displacement vectors are generally complex. This means that the left-hand side of equation 5 can be separated into the real and imaginary parts, which leads to coupled Christoffel equations for the vectors $\mathbf{m}$ and $\mathbf{U}$.

Carcione (2001) and Zhu and Tsvankin (2006) analyzed the Christoffel equation for attenuative anisotropic media (i.e., for complex c_{ijkl}), where the imaginary part $\mathbf{m}^{\text{im}}$ of the slowness vector is often assumed to be parallel to the real part $\mathbf{m}^{\text{re}}$ (wave propagation is then called "homogeneous"). The purpose of this

work, however, is to study evanescent waves for purely elastic (non-attenuative) models. When the medium is elastic and isotropic, the real and imaginary parts of the slowness vector are perpendicular to each other. Indeed, for a purely isotropic tensor c_{ijkl}, equation 5 reduces to (Tsvankin, 1995)

$$|\mathbf{m}^{\rm re}|^2 = \frac{1}{V^2} + |\mathbf{m}^{\rm im}|^2 \tag{6}$$

and

$$\mathbf{m}^{\rm re} \cdot \mathbf{m}^{\rm im} = 0\,, \tag{7}$$

where V is the velocity of P- or S-waves. According to equation 7, the direction of amplitude decay determined by $\mathbf{m}^{\rm im}$ is perpendicular to the wave-propagation direction $\mathbf{m}^{\rm re}$. The velocity of the evanescent wave from equation 3, which is equal to $1/|\mathbf{m}^{\rm re}|$, is always smaller than the medium velocity V (equation 6).

Below I treat evanescent waves that propagate in the horizontal plane $[x_1, x_2]$ and decay in the vertical direction x_3. Plane evanescent waves of this type are contained in Weyl-type integrals (i.e., in plane-wave decompositions of point-source radiation) used to solve reflection/transmission problems for horizontal interfaces (Tsvankin and Chesnokov, 1990; Tsvankin, 1995, 2005). The medium is assumed to be transversely isotropic with a vertical symmetry axis (VTI), but the results are also valid in the symmetry planes of HTI (TI with a horizontal symmetry axis) and orthorhombic media where the Christoffel equation has the same form as for vertical transverse isotropy (Tsvankin, 2005).

Since VTI media are azimuthally isotropic and all vertical planes are equivalent, it is sufficient to consider the slowness vector confined to the coordinate plane $[x_1, x_3]$ (i.e., $m_2 = 0$):

$$\mathbf{m}^{\rm re} = \{m_1^{\rm re}, 0, 0\}\,, \quad \mathbf{m}^{\rm im} = \{0, 0, m_3^{\rm im}\}\,. \tag{8}$$

Then the plane wavefrom equation 3 takes the form

$$u_n = U_n\, e^{i\omega(m_1 x_1 - t) - \omega m_3 x_3}\,. \tag{9}$$

Substituting the stiffness tensor for VTI media (e.g., Helbig, 1994) and the slowness vector from equation 8 into the Christoffel equation 5 yields

$$[c_{11}(m_1^{\rm re})^2 - c_{55}(m_3^{\rm im})^2 - \rho\,]\,U_1 + i(c_{13}+c_{55})\,m_1^{\rm re}\,m_3^{\rm im}\,U_3 = 0\,, \tag{10}$$

$$[c_{66}(m_1^{\rm re})^2 - c_{55}(m_3^{\rm im})^2 - \rho\,]\,U_2 = 0\,, \tag{11}$$

$$i(c_{13}+c_{55})\,m_1^{\rm re}\,m_3^{\rm im}\,U_1 + [c_{55}(m_1^{\rm re})^2 - c_{33}(m_3^{\rm im})^2 - \rho\,]\,U_3 = 0\,. \tag{12}$$

For brevity, henceforth the superscripts "re" and "im" are omitted because the horizontal component of $\mathbf{m}$ is real, while the vertical component is imaginary.

Exact solution for SH-waves

Since the slowness vector lies in a symmetry plane, SH-waves described by equation 11 are decoupled from in-plane polarized P- and SV-waves [equations 10 and 12]. The SH-wave polarization vector is orthogonal to the propagation plane $[x_1, x_3]$, and the horizontal and vertical slownesses are related by [equation 11]

$$c_{66}\,m_1^2 - c_{55}\,m_3^2 - \rho = 0\,. \tag{13}$$

The horizontal slowness in equation 13 can be expressed through the real part of the vertical slowness as

$$m_1^2 = \frac{1}{V_{\rm hor,SH}^2} + \frac{c_{55}}{c_{66}}\,m_3^2 = \frac{1}{1+2\gamma}\,\left(\frac{1}{V_{S0}^2} + m_3^2\right)\,, \tag{14}$$

where $\gamma \equiv (c_{66}-c_{55})/(2c_{55})$ is the Thomsen anisotropy parameter responsible for SH-wave anisotropy, $V_{S0} = \sqrt{c_{55}/\rho}$ is the shear-wave vertical velocity, and $V_{\rm hor,SH}$ is the horizontal velocity of homogeneous SH-waves:

$$V_{\rm hor,SH} = \sqrt{\frac{c_{66}}{\rho}} = V_{S0}\,\sqrt{1+2\gamma}\,. \tag{15}$$

Setting $\gamma = 0$ makes equation 14 identical to the corresponding isotropic expression 6. When the medium is anisotropic, the contribution of γ may substantially distort the dependence of the horizontal slowness m_1 on the vertical decay factor (slowness) m_3. Since typically $\gamma > 0$, it increases the value of m_3^2 (and, therefore, the decay factor) for a fixed horizontal slowness m_1.

Solutions for P- and SV-waves

In the following, the discussion is focused on evanescent P- and SV-waves. Equations 10 and 12 cannot be solved simultaneously with a real displacement (polarization) vector $\mathbf{U}$. Physically, this means that there is a phase shift between the vertical and horizontal polarization (displacement) components, and the polarization of evanescent waves is nonlinear. By analogy with known solutions for isotropic media (Tsvankin, 1995), this phase shift can be set to 90°, which corresponds to elliptical polarization. For simplicity, the horizontal component U_1 is taken to be real and the vertical component U_3 imaginary. However, since equations 10 and 12 constrain only the *ratio* of the polarization components, both U_1 and U_3 can be complex, as long as their phase factors differ by ±90°. As shown below, introducing a 90° phase shift between the polarization components is indeed sufficient to solve for the slownesses and polarizations of both P- and SV-waves.

If U_1 is real and $U_3 = i|U_3|$, equations 10 and 12 become

$$(c_{11}m_1^2 - c_{55}m_3^2 - \rho)\,U_1 - (c_{13}+c_{55})\,m_1 m_3\,|U_3| = 0\,, \tag{16}$$

$$(c_{13}+c_{55})\,m_1 m_3\,U_1 + (c_{55}m_1^2 - c_{33}m_3^2 - \rho)\,|U_3| = 0\,. \tag{17}$$

To obtain a non-trivial solution, the determinant of the

2×2 matrix formed by the coefficients multiplied with U_1 and U_3 has to be set to zero:

$$(c_{11}m_1^2 - c_{55}m_3^2 - \rho)\,(c_{55}m_1^2 - c_{33}m_3^2 - \rho) + (c_{13} + c_{55})^2\, m_1^2\, m_3^2 = 0\,. \quad (18)$$

Note that equation 18 becomes identical to the conventional equation for the slownesses of homogeneous P- and SV-waves in VTI media (e.g., Helbig, 1994) if m_3^2 is replaced by $-m_3^2$. As is the case for homogeneous waves, the slowness components m_1 and m_3 can be related to each other by solving a quadratic equation that follows from equation 18. Such solutions play an important role in deriving reflection/transmission coefficients (e.g., Rüger, 2001) because all waves scattered at a horizontal interface have the same horizontal slowness according to Snell's law.

Weak-anisotropy approximation for P-waves

Relationship between the slownesses

The exact expression for $m_1(m_3)$ (or vice versa) is rather involved and does not reveal the contributions of the anisotropy parameters. As shown in Appendix A, a simple approximation can be obtained by applying perturbation approach and linearizing equation 18 in Thomsen's (1986) parameters ϵ and δ. Henceforth, m_3 will be treated as a positive quantity, although (depending on the sign of x_3) it can become negative to ensure exponential amplitude decay of the evanescent wave in equation 9.

For the P-wave (i.e., for the solution with the smaller value of $|m_1|$ for a given $|m_3|$), the approximate horizontal slowness is given by

$$m_1^2 = \frac{1}{V_{\rm hor}^2} + m_3^2\,(1 - 4\epsilon + 2\delta) - 2m_3^4\,V_{P0}^2\,(\epsilon - \delta)\,, \quad (19)$$

where V_{P0} and $V_{\rm hor} = V_{P0}\,\sqrt{1+2\epsilon}$ are the vertical and horizontal velocities (respectively) of homogeneous P-waves with $m_3 = 0$. In the absence of anisotropy ($\epsilon = \delta = 0$), equations 18 and 19 become equivalent to the general isotropic expression 6:

$$m_1^2 = \frac{1}{V_{P0}^2} + m_3^2\,. \quad (20)$$

According to equation 20, m_1 monotonically increases with m_3, so the horizontal velocity of evanescent waves decreases from V_{P0} to zero as their amplitude decays faster in the vertical direction (see equation 9). It follows from equation 19 that this general trend is preserved in the presence of moderate anisotropy (also, see the numerical examples below).

Still, even relatively small values of the parameters ϵ and δ may significantly change the velocity $V_{\rm hor}$ and the m_3^2-term in equation 19, while the m_3^4-term is purely anisotropic. The multiplier of ϵ in the m_3^2-term is twice as large as that of δ because ϵ governs the P-wave velocity for near-horizontal directions. To separate the contribution of anisotropy to the linearized function $m_1(m_3)$, equation 19 can be rewritten as

$$\frac{m_1^2}{1/V_{P0}^2 + m_3^2} = 1 - 2\epsilon - 2m_3^2\,V_{P0}^2\,(\epsilon - \delta)\,. \quad (21)$$

For evanescent waves with small values of $m_3\,V_{P0}$ (i.e., with a slow amplitude decay), the anisotropic term in equation 21 is controlled primarily by ϵ. Since for typical TI models $\epsilon > 0$ and $\epsilon > \delta$, the influence of anisotropy reduces m_1 for a fixed value of m_3. This also means that for a given horizontal slowness m_1, anisotropy increases m_3 and, therefore, the amplitude decay factor.

The above results indicate that the relationship between m_1 and m_3 can help in constraining the anisotropy parameters ϵ and δ; this issue is addressed in more detail below.

Numerical examples

To evaluate the accuracy of the approximate relationship between m_1 and m_3, it is compared with the exact solution for a representative set of VTI models. Numerical tests in Figures 2 and 3 show that the error of equation 19 strongly depends on the magnitude of the difference $\epsilon - \delta$, which quantifies the deviation from elliptical anisotropy. The weak-anisotropy approximation remains accurate even for strongly anisotropic elliptical models with equal values of ϵ and δ (Figure 3). However, when $\epsilon > \delta$, the m_3^4-term in equation 19 rapidly increases with m_3 and may yield unphysical values of m_1 smaller than $1/V_{\rm hor}$ (see the model with $\epsilon = 0.4$ and $\delta = 0.1$ in Figure 3). Note that P-wave time processing in VTI media is controlled by the anellipticity parameter $\eta = (\epsilon - \delta)/(1+2\delta) \approx \epsilon - \delta$ (Alkhalifah and Tsvankin, 1995).

Predictably, for a constant $\epsilon - \delta$, the error of the weak-anisotropy approximation increases with the absolute values of both anisotropy parameters. However, for typical moderately anisotropic models (Figure 2b), equation 19 is sufficiently close to the exact solution when m_3 is relatively small and correctly reproduces the general trend of the function $m_1(m_3)$.

The above comparison of the exact and approximate solutions indicates that the linearized equation somewhat overstates the anisotropic contribution to the dependence of m_1 on m_3. Still, for typical models with $\epsilon > 0$ and $\epsilon - \delta \geq 0$, the anisotropic terms substantially reduce the slowness m_1 for a fixed value of m_3, as predicted by the weak-anisotropy approximation 19 (Figure 4). In agreement with the exact expression 14 for elliptical anisotropy, the ratio of the VTI and isotropic values of m_1 is independent of m_3 when $\epsilon = \delta$ (Figure 4a). For models with $\epsilon - \delta > 0$ (Figure 4b), the difference between the VTI and isotropic results becomes more pronounced for larger values of m_3, which correspond to slower evanescent waves with a higher rate of amplitude decay.

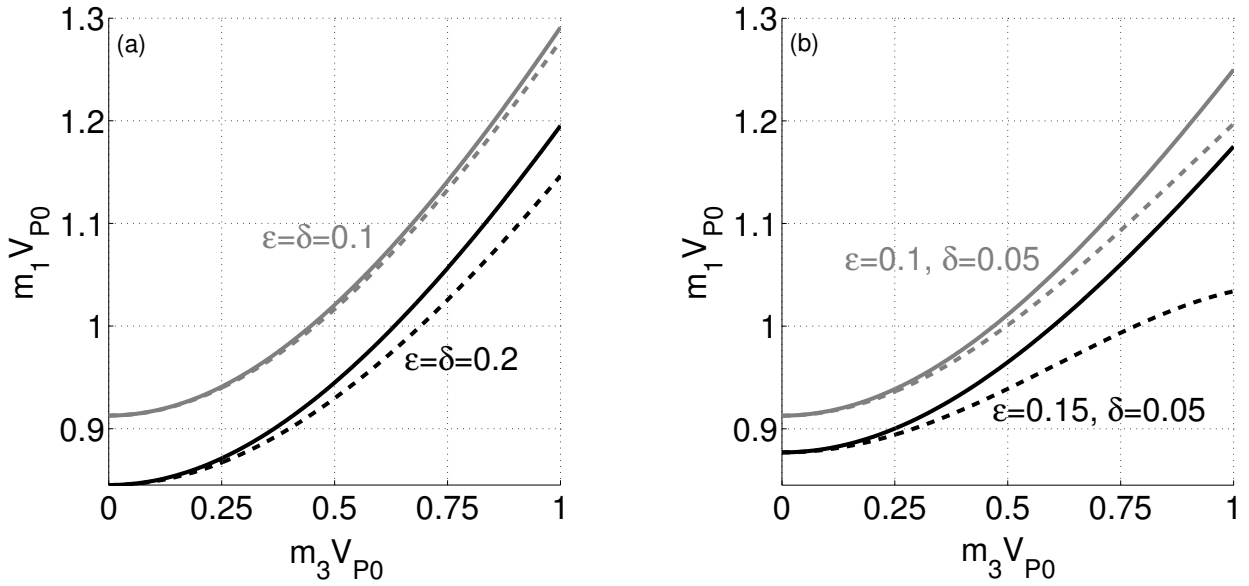

Figure 2. Comparison of the exact function $m_1(m_3)$ from equation 18 (solid curves) with the weak-anisotropy approximation 19 (dashed) for elliptical (a) and nonelliptical (b) VTI models. The error of the approximation becomes larger with increasing values of $\epsilon - \delta$. Both slowness components are multiplied with the velocity V_{P0} to make them dimensionless.

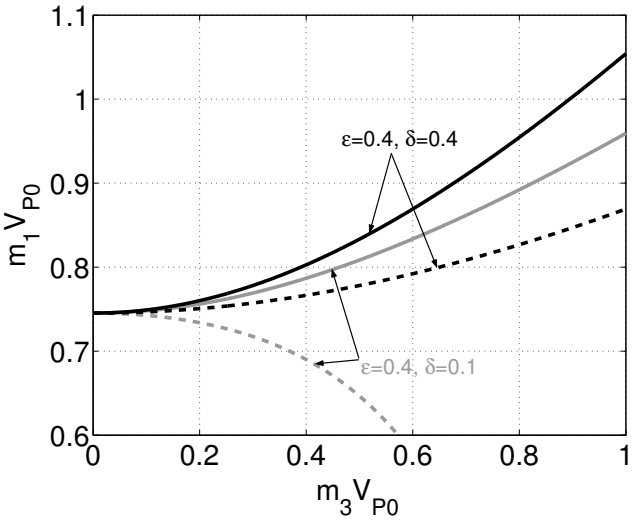

Figure 3. Comparison of the exact (solid curves) and approximate (dashed) functions $m_1(m_3)$ for two models with strong velocity anisotropy.

Polarization ellipse

Substitution of m_1 from equation 19 into equations 16 or 17 yields the ratio of the polarization components U_1 and U_3, which determines the eccentricity of the polarization ellipse. Linearizing the result in the anisotropy parameters and the V_{S0}/V_{P0} ratio yields

$$\frac{|U_3|}{|U_1|} = \frac{m_3\, V_{P0}}{\sqrt{1+m_3^2\, V_{P0}^2}} \left[1-(\epsilon-\delta)(1+m_3^2\, V_{P0}^2)\right] . \quad (22)$$

For a homogeneous P-wave with $m_3 = 0$, the displacement vector is horizontal ($U_3 = 0$), so the wave is polarized in the direction of propagation. The polarization becomes nonlinear with increasing m_3, and the anisotropic term that involves $\epsilon-\delta$ can make a substantial contribution to the polarization ellipse. Since typically $\epsilon-\delta > 0$, the influence of anisotropy in equation 22 reduces the ratio $|U_3|/|U_1|$ and makes the polarization more linear.

Weak-anisotropy approximation for SV-waves

Relationship between the slownesses

In principle, the approximate horizontal slowness for SV-waves can be derived in the same way as the one for P-waves by perturbing the isotropic expression for $m_1(m_3)$. Such a derivation, however, is unnecessary because any linearized kinematic (i.e., based entirely on slowness or velocity) signature for SV-waves can be obtained directly from the corresponding P-wave expression by making the following substitutions (Tsvankin, 2005): V_{P0} has to be replaced with V_{S0}, δ with the SV-wave velocity parameter $\sigma \equiv (V_{P0}^2/V_{S0}^2)\,(\epsilon-\delta)$, and ϵ set to zero. Applying this recipe to equation 19 leads to

$$\begin{aligned} m_1^2 &= \frac{1}{V_{S0}^2} + m_3^2\,(1+2\sigma) + 2m_3^4\, V_{S0}^2\,\sigma \\ &= \frac{1}{V_{S0}^2} + m_3^2\,(1+2\sigma) + 2m_3^4\, V_{P0}^2\,(\epsilon-\delta) . \end{aligned} \quad (23)$$

Anisotropy does not change the horizontal velocity of homogeneous SV-waves (it corresponds to $m_3 = 0$),

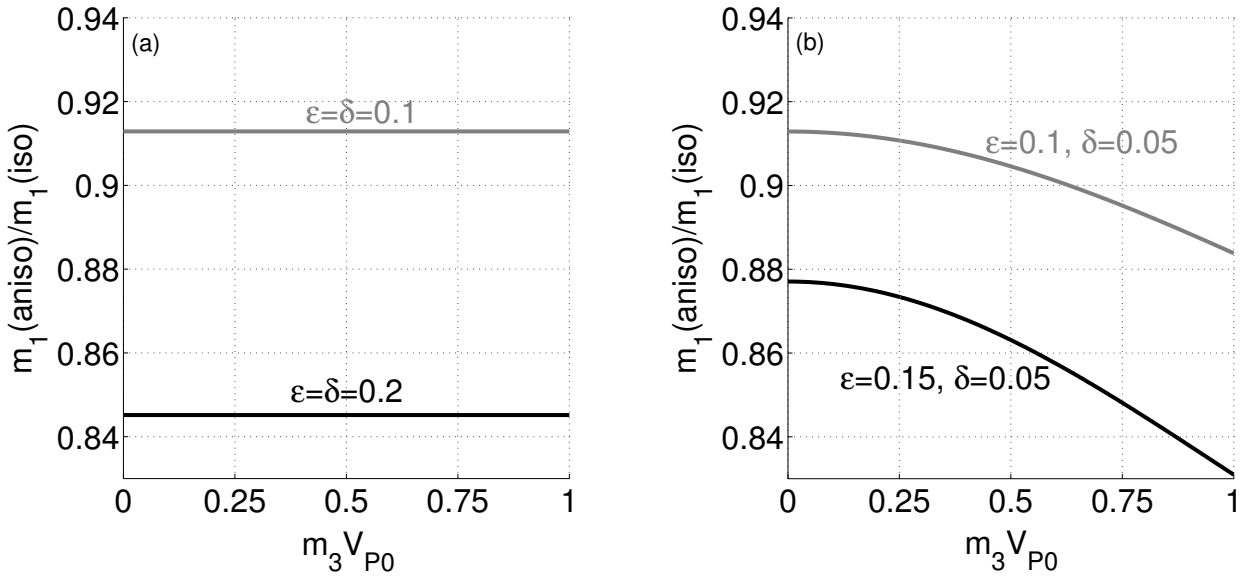

Figure 4. Influence of anisotropy on the relationship between the horizontal and vertical slownesses for the models from Figure 2. The exact slowness m_1 computed from equation 18 is normalized by the isotropic value that corresponds to $\epsilon = \delta = 0$. The shape of the normalized curves is qualitatively described by the weak-anisotropy approximation 21.

which is equal to the vertical velocity V_{S0}. Since the parameter σ typically is positive (Tsvankin, 2005), its influence reduces m_3 and the amplitude decay factor for a fixed value of m_1. Because of the presence of the squared vertical-velocity ratio, the average value of σ for such common TI formations as shales exceeds 0.5 (Wang, 2002). Therefore, the contribution of the anisotropy to the m_3^2-term is even more substantial for SV-waves than for P-waves. It is interesting that the factor $1 + 2\sigma$ in equation 23 is also responsible for the SV-wave NMO velocity in VTI media (Thomsen, 1986).

Polarization ellipse

The linearized polarization ellipse for evanescent SV-waves has the form

$$\frac{|U_1|}{|U_3|} = \frac{m_3\, V_{S0}}{\sqrt{1 + m_3^2\, V_{S0}^2}} \left[1 - (2\epsilon - \delta) - 2\sigma\, m_3^2\, V_{S0}^2\right] . \quad (24)$$

The polarization vector for a homogeneous SV-wave ($m_3 = 0$) is vertical; the horizontal displacement component increases with m_3. According to equation 24, the anisotropic terms typically reduce the ellipticity of the SV-wave polarization, which was also the case for P-waves.

Discussion and conclusions

Evanescent waves play an important role in a number of wave-propagation problems, such as generation of nongeometrical modes by sources located close to medium interfaces. This paper introduces concise weak-anisotropy approximations for the slowness and polarization vectors of evanescent plane waves that propagate in the horizontal plane of VTI media and decay in the vertical direction. The results remain entirely valid in the symmetry planes of azimuthally anisotropic models with HTI and orthorhombic symmetry.

The velocity of evanescent waves can take any value smaller than the horizontal velocity of the corresponding (i.e., P, SV, or SH) homogeneous wave. By solving the Christoffel equation, one can relate the evanescent-wave velocity (or the horizontal slowness m_1) to the vertical slowness m_3, which governs the amplitude decay factor. While the exact relationship between m_1 and m_3 for SH-waves is rather simple and involves a single anisotropy parameter (γ), it is much less transparent for P- and SV-waves. To explain the contribution of anisotropy to both the slowness and polarization vectors of evanescent P- and SV-waves, the solutions of the Christoffel equation were linearized in the parameters ϵ and δ.

The anisotropic terms in the approximate P-wave function $m_1(m_3)$ include both ϵ and δ, although the sensitivity to ϵ is higher. Most importantly, even for relatively small values of ϵ and δ on the order of 0.1–0.15, the influence of anisotropy on the relationship between m_1 and m_3 is significant, especially for evanescent waves with smaller velocities and higher amplitude decay rates. For typical VTI models with $\epsilon > 0$ and $\epsilon > \delta$, the decay factor governed by m_3 can be much larger than that in isotropic media for the same value of m_1. Numerical testing demonstrates that the accuracy of the weak-anisotropy approximation for the de-

pendence $m_1(m_3)$ is mostly governed by the difference $\epsilon - \delta$, rather than by either parameter individually.

The linearized relationship $m_1(m_3)$ for SV-waves was obtained as a special case of the P-wave result by applying the "substitution rule" described in Tsvankin (2005) for homogeneous waves. In contrast to P-waves, the influence of anisotropy reduces the amplitude decay factor of SV-waves for a given m_1. The anisotropic terms in the function $m_1(m_3)$ are controlled by the SV-wave velocity parameter σ, which often reaches large values exceeding 0.5.

The polarization of evanescent P- and SV-waves becomes increasingly nonlinear (elliptical) with a reduction in their horizontal velocity. The weak-anisotropy approximation for the ratio of the vertical and horizontal displacements shows that for both P- and SV-waves the contribution of ϵ and δ typically decreases the eccentricity of the polarization ellipse.

These results will help to develop asymptotic solutions for nongeometrical waves in anisotropic media using, for example, the stationary-phase method. In particular, the description of evanescent waves given above is directly applicable to leaking waves (Figure 1) excited by buried (e.g., borehole) sources at internal boundaries. The dependence of the horizontal velocity on the amplitude decay factor of evanescent waves can be directly measured by recording leaking waves in cross-hole or reverse VSP (vertical seismic profiling) surveys; for examples, see Tsvankin (1995). To estimate the decay factor of a leaking wave, the source should be moved along the borehole while keeping the receiver position fixed. The strong influence of the anisotropy parameters on the function $m_1(m_3)$ indicates that leaking modes can be effectively used to constrain anisotropic velocity fields.

Acknowledgments

I am grateful to my colleagues at the Center for Wave Phenomena (CWP), Colorado School of Mines (CSM), for useful discussions and to Jyoti Behura (CSM) for help with the numerical examples. Reviews by Roel Snieder and Yaping Zhu (both CSM) helped to improve the manuscript. The support for this work was provided by the Consortium Project on Seismic Inverse Methods for Complex Structures at CWP and by the Chemical Sciences, Geosciences and Biosciences Division, Office of Basic Energy Sciences, Office of Science, U.S. Department of Energy.

REFERENCES

Aki, K., and P. G. Richards, 1980, Quantitative seismology. Theory and methods: W. N. Freeman & Co.

Alkhalifah, T., and I. Tsvankin, 1995, Velocity analysis in transversely isotropic media: Geophysics, **60**, 1550–1566.

Brekhovskikh, L. M., 1980, Waves in layered media: Academic Press.

Carcione, J. M., 2001, Wave fields in real media: Wave propagation in anisotropic, anelastic, and porous media: Pergamon Press.

Crampin, S., 1975, Distinctive particle motion of surface waves as a diagnostic of anisotropic layering: Geophysical Journal of the Royal Astronomical Society, **40**, 177–186.

Crampin, S., and D. B. Taylor, 1971, The propagation of surface waves in anisotropic media: Geophysical Journal of the Royal Astronomical Society, **25**, 71–87.

Grechka, V., A. Pech, and I. Tsvankin, 2002a, P–wave stacking-velocity tomography for VTI media: Geophysical Prospecting, **50**, 151–168.

Helbig, K., 1994, Foundations of elastic anisotropy for exploration seismics: Pergamon Press.

Hron, F., and B. G. Mikhailenko, 1981, Numerical modeling of nongeometrical effects by the Alekseev-Mikhailenko method: Bulletin of the Seismological Society of America, **71**, 1011–1029.

Rüger, A., 2001, Reflection coefficients and azimuthal AVO analysis in anisotropic media: Society of Exploration Geophysicists.

Thomsen, L., 1986, Weak elastic anisotropy: Geophysics, **51**, 1954–1966.

Tsvankin, I., 1995, Seismic wavefields in layered isotropic media: Samizdat Press, Colorado School of Mines.

Tsvankin, I., 2005, Seismic signatures and analysis of reflection data in anisotropic media: Elsevier Science Publ. Co., Inc (second edition).

Tsvankin, I., and Chesnokov, E., 1990, Synthesis of body wave seismograms from point sources in anisotropic media: Journal of Geophysical Research, **95(B7)**, 11317–11331.

Wang, Z., 2002, Seismic anisotropy in sedimentary rocks, part 2: Laboratory data: Geophysics, **67**, 1423–1440.

Zhu, Y., and I. Tsvankin, 2006, Plane-wave propagation in attenuative TI media: Geophysics, in print.

APPENDIX A: LINEARIZED RELATIONSHIP BETWEEN THE SLOWNESSES OF EVANESCENT WAVES

The horizontal slowness m_1 of evanescent waves can be expressed as a function of the imaginary part m_3 of the vertical slowness (m_3 represents the frequency-normalized decay factor) by solving equation 18. To develop the weak-anisotropy approximation for the function $m_1(m_3)$, it is convenient to replace the stiffness coefficients in equation 18 by the parameters ϵ and δ:

$$c_{11} = V_{P0}^2\,\rho\,(1+2\epsilon)\,, \tag{A1}$$

$$c_{33} = V_{P0}^2\,\rho\,, \tag{A2}$$

$$c_{55} = V_{S0}^2\,\rho\,, \tag{A3}$$

$$(c_{13}+c_{55})^2 = V_{P0}^4\,\rho^2\,f\,(2\delta+f)\,, \tag{A4}$$

where $f \equiv 1 - V_{S0}^2/V_{P0}^2$ is a useful parameter combination introduced into TI velocity equations by Tsvankin (2005).

The isotropic solutions for $m_1(m_3)$ are obtained by setting $\epsilon = \delta = 0$ and substituting equations A1–A4 into equation 18:

$$m_1^2 = \frac{1}{V^2} + m_3^2\,, \tag{A5}$$

with the medium velocity V equal to V_{P0} for P-waves and V_{S0} for S-waves.

The weak-anisotropy approximation can be derived by perturbing the isotropic expression A5. For P-waves, such a perturbation can be written as

$$m_1^2 = \frac{1}{V_{P0}^2} + m_3^2 + \Delta(m_1^2)\,, \tag{A6}$$

where $\Delta(m_1^2)$ is a linear function of ϵ and δ. Substituting m_1^2 from equation A6 into equation 18 and keeping only the linear terms in the anisotropy parameters yields

$$\Delta(m_1^2) = -2\epsilon\,\frac{(1+m_3^2\,V_{P0}^2)^2}{V_{P0}^2} + 2\delta\,m_3^2\,(1+m_3^2\,V_{P0}^2)\,. \tag{A7}$$

The linearized approximation for m_1^2 is then obtained from equation A6 as

$$m_1^2 = \frac{1}{V_{\rm hor}^2} + m_3^2\,(1-4\epsilon+2\delta) - 2m_3^4\,V_{P0}^2\,(\epsilon-\delta)\,; \tag{A8}$$

$V_{\rm hor} = V_{P0}\,\sqrt{1+2\epsilon}$ is the P-wave horizontal velocity.